Multilevel Regulation of NF-κB Signaling by NSD2 Suppresses *Kras*-Driven Pancreatic Tumorigenesis

Wenxin Feng, Ningning Niu, Ping Lu, Zhuo Chen, Hanyu Rao, Wei Zhang, Chunxiao Ma, Changwei Liu, Yue Xu, Wei-Qiang Gao, Jing Xue,* and Li Li*

Pancreatic ductal adenocarcinoma (PDAC) is a clinically challenging cancer with a dismal overall prognosis. NSD2 is an H3K36-specific di-methyltransferase that has been reported to play a crucial role in promoting tumorigenesis. Here, the study demonstrates that NSD2 acts as a putative tumor suppressor in *Kras*-driven pancreatic tumorigenesis. NSD2 restrains the mice from inflammation and *Kras*-induced ductal metaplasia, while NSD2 loss facilitates pancreatic tumorigenesis. Mechanistically, NSD2-mediated H3K36me2 promotes the expression of IκBα, which inhibits the phosphorylation of p65 and NF-κB nuclear translocation. More importantly, NSD2 interacts with the DNA binding domain of p65, attenuating NF-κB transcriptional activity. Furthermore, inhibition of NF-κB signaling relieves the symptoms of *Nsd2*-deficient mice and sensitizes *Nsd2*-null PDAC to gemcitabine. Clinically, NSD2 expression decreased in PDAC patients and negatively correlated to nuclear p65 expression. Together, the study reveals the important tumor suppressor role of NSD2 and multiple mechanisms by which NSD2 suppresses both p65 phosphorylation and downstream transcriptional activity during pancreatic tumorigenesis. This study opens therapeutic opportunities for PDAC patients with *NSD2* low/loss by combined treatment with gemcitabine and NF-κBi.

1. Introduction

Pancreatic ductal adenocarcinoma (PDAC) is a deadly disease that is estimated to become the second-leading cause of cancer death in the US by 2030 at a rate of 0.5% to 1.0% per year.[1,2] In 90% of cases, pancreatic cancer is discovered at a late stage, when it has spread beyond the pancreas, and over half have metastasized to other organs.[2,3] Multiple genetic alterations are involved in the pathophysiology of PDAC, including *KRAS, TP53, SMAD4,* and *CDKN2A*,[4] and *KRAS* variants are identified in 90% to 92% of individuals with PDAC.[4] Mouse models expressing *Kras* variants in acinar cells typically develop distinct precursor lesions known as pancreatic intraepithelial neoplasia (PanIN).

Nuclear factor kappa-light-chain-enhancer of activated B cells (NF-κB) is a transcription factor and key inducer of inflammatory responses.[5] One of the major subunits of NF-κB, RelA (p65), forms heterodimers with the structurally related p50 protein.[6] In the canonical pathway, most p65-p50 heterodimers are located within the cytoplasm under basal conditions due to its association with inhibitors of NF-κB, IκBα. Stimulation of cells with NF-κB-activating ligands such as the cytokine tumor necrosis factor (TNF) results in the degradation of IκBα, and then NF-κB translocates to the nucleus, where it regulates transcriptional programs.[7] Studies have shown that NF-κB signaling is constitutively activated in almost 70% of pancreatic cancer specimens[8] and plays a crucial role in PDAC development, progression, and resistance.[9]

Pancreatic tumorigenesis is also mediated by epigenetic regulation, which includes DNA methylation, histone modifications,

W. Feng, H. Rao, W. Zhang, C. Ma, C. Liu, Y. Xu, W.-Q. Gao, L. Li
State Key Laboratory of Systems Medicine for Cancer
Renji-Med X Clinical Stem Cell Research Center
Ren Ji Hospital
School of Medicine and School of Biomedical Engineering
Shanghai Jiao Tong University
Shanghai 200127, China
E-mail: lil@sjtu.edu.cn

W. Feng, Z. Chen, H. Rao, W. Zhang, C. Ma, C. Liu, Y. Xu, W.-Q. Gao, L. Li
School of Biomedical Engineering and Med-X Research Institute
Shanghai Jiao Tong University
Shanghai 200030, China

N. Niu, P. Lu, J. Xue
State Key Laboratory of Systems Medicine for Cancer
Stem Cell Research Center
Ren Ji Hospital
Shanghai Cancer Institute
Shanghai Jiao Tong University School of Medicine
Shanghai 200127, China
E-mail: jingxue@sjtu.edu.cn

**ADVANCED
SCIENCE NEWS**

www.advancedsciencenews.com

**ADVANCED
SCIENCE**
Open Access

www.advancedscience.com

and chromatin remodeling.[10–12] Recent study revealed that SETD2-H3K36me3 deficiency can reprogram neutrophils to an immunosuppressive phenotype, thereby promoting immune escape during pancreatic tumor progression.[13] In addition, histone methyltransferase EZH2 can regulate PDAC plasticity, dedifferentiation, and molecular subtype identity.[14] NSD2 is a histone methyltransferase that can catalyze the di-methylation of histone H3 at lysine 36 (H3K36me2), a permissive mark associated with active gene transcription.[15–17] NSD2 has been reported to be amplified, mutated, or overexpressed in human cancers. The NSD2 t (4;14) chromosomal translocation in multiple myeloma is associated with the overexpression of NSD2 and leads to a poor prognosis.[18,19] NSD2 is overexpressed in invasive prostate cancer, especially in metastases, and is associated with the poor prognosis of prostate cancer patients.[20] Similar results have also been reported in other tumor types, such as esophageal carcinoma, stomach carcinoma, hepatocellular carcinoma, lung cancer, and corpus uteri malignancy, etc.[17] Many studies have identified that NSD2 promotes cell proliferation, migration, invasion, and epithelial-mesenchymal transformation (EMT), proving that it plays a crucial oncogenic role[15–17] However, the mechanism of NSD2 in pancreatic tumorigenesis remains unclear.

In this study, we investigated the role of NSD2 in *Kras*-induced pancreatic tumorigenesis. We found that NSD2 overexpression inhibited inflammation and *Kras*-induced ductal metaplasia in mice, whereas NSD2 loss facilitated *Kras*-induced tumorigenesis. Our results demonstrate that NSD2-mediated H3K36me2 promotes the expression of IκBα, inhibiting the phosphorylation of p65. More importantly, NSD2 interacts with the DNA binding domain of the NF-κB p65 protein, attenuating NF-κB transcriptional activity. Therefore, we uncovered multilevel regulation of NF-κB signaling by NSD2 during pancreatic tumorigenesis.

2. Results

2.1. NSD2 Overexpression Restrains Pancreatic Ductal Metaplasia Induced by Inflammation and/or *Kras* Mutation

To assess the role of NSD2 in pancreatic tumorigenesis, we generated pancreatic-specific NSD2-overexpressing mice together with oncogenic *Kras* mutation. Mice harboring a single copy of a minigene consisting of a CAGGS (a hybrid chicken β-actin and cytomegalovirus) promoter, a loxP-STOP-loxP (LSL) cassette, and Myc-tagged *Nsd2* cDNA knocked into the Rosa26 locus (*Nsd2*[OE/+])[20] were crossed with *Pdx*[Cre]; LSL-*Kras*[G12D] mice (referred to as PK mice) to obtain *Pdx*[Cre]; LSL-*Kras*[G12D]; *Nsd2*[OE/+] mice (referred to as PKN° mice) (**Figure 1A**). The overexpression of NSD2 in the PKN° pancreas was verified by using Western blotting and immunohistochemistry (IHC) (Figure 1B,C). To investigate the biological function of NSD2 in the pancreas under the context of injury, we first applied a caerulein-induced pancreatitis recovery model (RAP) to 8-week-old PK and PKN° mice (100 µg kg^{-1}, 8 hourly injection/day) (Figure 1D). In comparison with PK mice, there were much less acinar-to-ductal metaplasia (ADM) lesions in the pancreata of PKN° mice on both day 7 and day 18, demonstrating that NSD2 overexpression significantly restrained the inflammation-induced ADM (Figure 1E,F). In addition, we compared the ductal lesions between PK and PKN° mice at 24 weeks of age to illustrate the impact of NSD2 overexpres-

sion on *Kras*-induced ductal metaplasia. Strikingly, PKN° mice showed significantly reduced development of ADM, PanIN, and PDAC lesions compared to PK mice (Figure 1G,H). Consistently, CK19$^+$ and Ki67$^+$ signals decreased dramatically in PKN° lesions (Figure 1I). Furthermore, pancreatic acinar explants derived from PKN° mice dedifferentiated less into ductal-like structures than explants from PK mice in response to transforming growth factor α (TGFα) (Figure 1J,K). Collectively, these findings indicate that NSD2 overexpression reinforces the acinar homeostasis and inhibits the pancreatic ductal metaplasia induced by both inflammation and *Kras*[G12D].

2.2. NSD2 Loss Facilitates *Kras*-Induced Ductal Metaplasia

We next aimed to determine whether NSD2 loss could promote pancreatic tumorigenesis. Previously described *Nsd2*[f/f] mice[20] were crossed with *Pdx*[Cre]; LSL-*Kras*[G12D] mice (PK mice) to ablate NSD2 in the pancreas (*Pdx*[Cre]; *Kras*[G12D]; *Nsd2*[f/f], referred to as PKN[f/f] mice). By using Western blotting, IHC, and Real-Time quantitative PCR (RT-qPCR), we found that the H3K36me2 level was unchanged in the pancreas of PKN[f/f] mice compared to PK mice, although *Nsd2* was thoroughly ablated (**Figure 2A–C**). This finding was inconsistent with previous studies, which manifested that *Nsd2* deletion reduced H3K36me2 levels in prostate cancer,[20,21] breast cancer,[22] osteosarcoma,[23] lung adenocarcinoma,[24] etc. The maintained H3K36me2 level could be elucidated by the fact that the expression levels of demethylases of the H3K36 site, including *Kdm2b*, *Kdm4a*, *Kdm4b*, and *No66*, were also significantly decreased in the *Nsd2*-deficient pancreas, and the expression level of *Nsd3* was significantly increased, while *Nsd1* expression remained unchanged (Figure 2C).

PK mice developed infrequent ADM lesions at 12 weeks of age and gradually progressed to low-grade panIN at ≈24 weeks of age (Figure 2D,E). In sharp contrast to age-matched PK mice, additional depletion of *Nsd2* accelerated the ductal metaplasia, and led to a more affected pancreatic area with much higher grades of PanIN/PDAC lesions at 24 weeks of age, along with enhanced cell proliferation (Figure 2E–G). We also found that pancreatic acinar explants derived from *Pdx*[Cre]; *Nsd2*[f/f] mice dedifferentiated more into ductal-like structures than those from control mice (*Nsd2*[f/f] mice) (Figure 2H). Collectively, *Nsd2* loss synergized with oncogenic *Kras* to facilitate ADM transition and progression toward PanIN and PDAC.

To further analyze the effects of NSD2 loss, we depleted *Nsd2* with CRISPR/Cas9 (Nsd2-KO) in KPC1199, a murine pancreatic cancer cell line derived from KPC mice (*Pdx*[Cre]; LSL-*Kras*[G12D]; LSL-*TP53*[R172H]) and human PDAC cell line ASPC1. Western blotting analyses showed a reduction in NSD2 but not H3K36me2 (Figure 2I). Consistent with the increased Ki67$^+$ proportion, CCK8 assays confirmed the increased cell proliferation under NSD2 loss (Figure 2J; Figure S2B, Supporting Information).

In line with the previous results (Figure 2C), the H3K36me2 level was also not impaired in *Nsd2*-deficient cells due to the decreased expression levels of the demethylases and increased expression level of *Nsd3* (Figure S2A, Supporting Information). Together, these results demonstrate that *Nsd2* deletion promotes cell proliferation and accelerates pancreatic tumorigenesis.
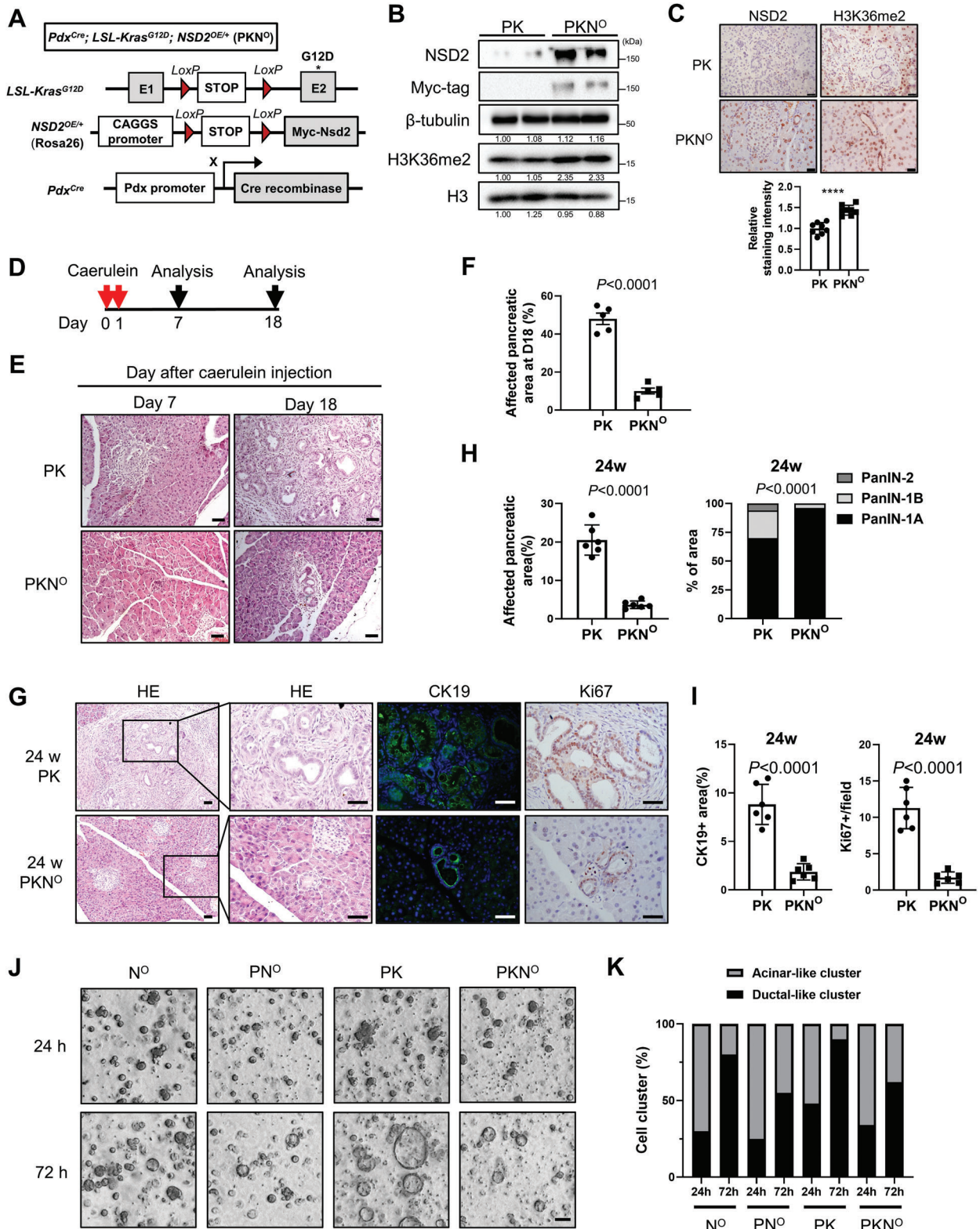
Figure 1. NSD2 overexpression restrains pancreatic ductal metaplasia induced by inflammation and / or *Kras* mutation. A) Construction and breeding strategy of *Pdx*^Cre^; LSL-*Kras*^G12D^; *Nsd2*^OE/+^ mice (PKN°). B) Western blotting analysis of NSD2 and H3K36me2 expression in pancreas tissues of PK and PKN° mice. Experiments were repeated at least three times, with similar results. C) IHC analysis of NSD2 and H3K36me2 expression in pancreas tissues of PK and PKN° mice. Quantification of H3K36me2 staining intensity is shown at the bottom. Experiments were repeated at least three times, with similar results, and representative images are shown. Scale bars: 25 μm. D,E) PK and PKN° mice were administrated with caerulein (100 μg kg⁻¹,

**ADVANCED
SCIENCE NEWS**

www.advancedsciencenews.com

**ADVANCED
SCIENCE**
Open Access

www.advancedscience.com

2.3. Loss of NSD2 Activates the NF-κB Signaling Pathway

To gain mechanistic insight into how NSD2 loss promotes pancreatic tumorigenesis, we conducted an expression profile analysis of control (Ctrl) and Nsd2-KO cells by RNA sequencing (RNA-seq) (**Figure 3**A). There were 296 upregulated and 203 downregulated genes on Nsd2 loss. Gene Ontology (GO) analysis indicated that NSD2 loss significantly enriched the genes associated with the positive regulation of NF-κB transcription factor activities and activation of NF-κB-inducing kinase activities (Figure 3B). To better understand NSD2-mediated signaling circuits, we performed GSEA, and the data showed that NSD2 loss significantly enriched the genes linked to TNFα signaling via NF-κB, E2F targets and inflammatory response (Figure 3C).

Next, we performed RNA-seq of pancreatic tissue isolated from PK and littermate PKN° mice (8 weeks old), and the analysis indicated that there were 632 upregulated and 963 downregulated genes. In line with the previous results, NF-κB signaling pathway was inhibited on Nsd2 overexpression (Figure S3A,B, Supporting Information).

To confirm that loss of NSD2 activates the NF-κB signaling pathway, Western blotting was performed to examine the protein levels of core members involved in canonical NF-κB signaling. The results showed that the phosphorylation of p65 was increased in Nsd2-KO cells, while the IκBα level decreased correspondingly (Figure 3D). The Western blotting assays showed the same results in mice, which indicates the activation of the NF-κB signaling pathway in the pancreatic tissue of PKN$^{f/f}$ mice (Figure 3E). Together, these results prove that loss of NSD2 activates the NF-κB signaling pathway.

To assess the function of NSD2 in human PDAC, we compared the transcriptome differences between NSD2^{high} (top 25% of *NSD2* mRNA level, 45 cases) and NSD2^{low} (bottom 25% of *NSD2* mRNA level, 45 cases) patients in TCGA (PAAD) databases (Figure 3F). We performed gene set enrichment analysis (GSEA) to gain a global view of the distinguished transcriptome profiles between NSD2^{high} and NSD2^{low} patients. Genes related to inflammatory response and TNFα signaling via NF-κB were significantly upregulated in PDAC with lower *NSD2* expression (Figure 3F,G). Taken together, these findings revealed the link between NSD2 reduction and the activation of NF-κB signaling.

2.4. NSD2 Promotes Nfkbia Expression and Inhibits p65 Nuclear Translocation

As shown in Figure 3D,E, depletion of Nsd2 increased the phosphorylation of p65 and decreased the protein level of IκBα, suggesting that NSD2/H3K36me2 might positively regulate the expression of *Nfkbia*, IκBα coding gene. As expected, the *Nfkbia* mRNA level was downregulated in PKN$^{f/f}$ mice, and up-

regulated in PKN° mice (Figure S4A, Supporting Information). Downregulated *Nfkbia* expression was further validated in *Nsd2*-deficient KPC1199 cells (Figure S4B, Supporting Information). Furthermore, an NSD2 mutant vector for enzymatic activities (a tyrosine to alanine substitution at amino acid Y1179 abolished NSD2 methylation of nucleosomes)[24] was applied (Figure S4C, Supporting Information). The results showed that Nsd2^{WT} overexpression increased the expression level of *Nfkbia*, while Nsd2^{Y1179A} cells failed to upregulate *Nfkbia* expression level (Figure S4D–F, Supporting Information), indicating that the methyltransferase activity of NSD2 is essential to promote *Nfkbia* expression.

To determine whether NSD2 inhibits the NFKBIA expression through H3K36me2, we conducted ChIP-seq (chromatin immunoprecipitation followed by high-throughput sequencing) to characterize the differences in the genomic distribution of H3K36me2 between empty vector (EV) and NSD2-overexpressing (Nsd2-OE) PDAC cells. In line with the notion that H3K36me2 modification is critical for gene transcription and elongation, the signals of H3K36me2 were significantly increased within the promoter areas and throughout gene bodies in Nsd2-OE cells, compared with EV cells (**Figure 4**A). As expected, we observed a significant increase in H3K36me2 signals in the *NFKBIA* gene locus, especially within the 5′-UTR and promoter regions in Nsd2-OE cells (Figure 4B).

Although NSD2 loss did not significantly reduce the H3K36me2 level (Figure 2A,B), we also examined the distribution patterns of H3K36me2 using ChIP-seq in Ctrl and Nsd2-KO cells (Figure S4G, Supporting Information). We observed a significant reduction in H3K36me2 signals in the *NFKBIA* gene locus, especially within the 5′-UTR and promoter regions (Figure S4H, Supporting Information).

We further confirmed the existence of H3K36me2 marks at the promoter of the *Nfkbia* gene by ChIP-qPCR, and the signals decreased along with *Nsd2* loss (Figure 4C). Consistent with the previous results, the intensity of H3K36me2 bindings of the *Nfkibia* promoter increased in Nsd2^{WT} cells, rather than in Nsd2^{Y1179A} cells (Figure 4C). These data demonstrated that NSD2-mediated H3K36me2 directly regulates the expression of *Nfkbia*. Clinically, we found a strong correlation between *NSD2* and *NFKBIA* mRNA levels based on human GTEx-Pancreas database (Figure 4D). To clarify the functional importance of the NSD2/NFKBIA axis, we overexpressed NFKBIA in Nsd2-deficient cells and found that NFKBIA overexpression diminished p65 phosphorylation in Nsd2-deficient cells (Figure 4E). Together, our results indicate that NSD2-mediated H3K36me2 promotes the expression of IκBα, which inhibits the phosphorylation of p65.

Activation of the canonical NF-κB pathway leads to nuclear translocation of the p65-p50 dimer, which functions as a transcriptional activator.[5] We next explored whether *Nsd2* deletion

8 hourly injection/day) for consecutive 2 days. Pancreas tissues were collected at indicated days for HE staining (n = 5 per group). Scale bars: 50 μm. F) Quantification of affected pancreatic area (%) in pancreas tissue from indicated mice at day 18 (n = 5 per group). G) Pancreatic tissues from indicated mice for staining of HE, CK19, and Ki67 (n = 6 per group). Scale bars: 50 μm. H) Quantification of affected pancreatic area (%) and the ratio of PanIN-1A, PanIN-1B, and PanIN-2 in affected pancreatic areas from indicated mice at 24 weeks (n = 6 per group). I) Quantification of CK19 positive area and Ki67 positive cells per field from indicated mice at 24 weeks (n = 6 per group). J,K) Representative images and statistic of acinar-to-ductal metaplasia of acinar explants on transforming growth factor α (TGFα) stimulation from indicated mice. *Nsd2*$^{OE/+}$ referred to as N°. *Pdx*^{Cre}; *Nsd2*$^{OE/+}$ mice referred to as PN°. Experiments were repeated at least three times, with similar results, and representative images are shown. Scale bars: 50 μm.

ADVANCED
SCIENCE NEWS

www.advancedsciencenews.com

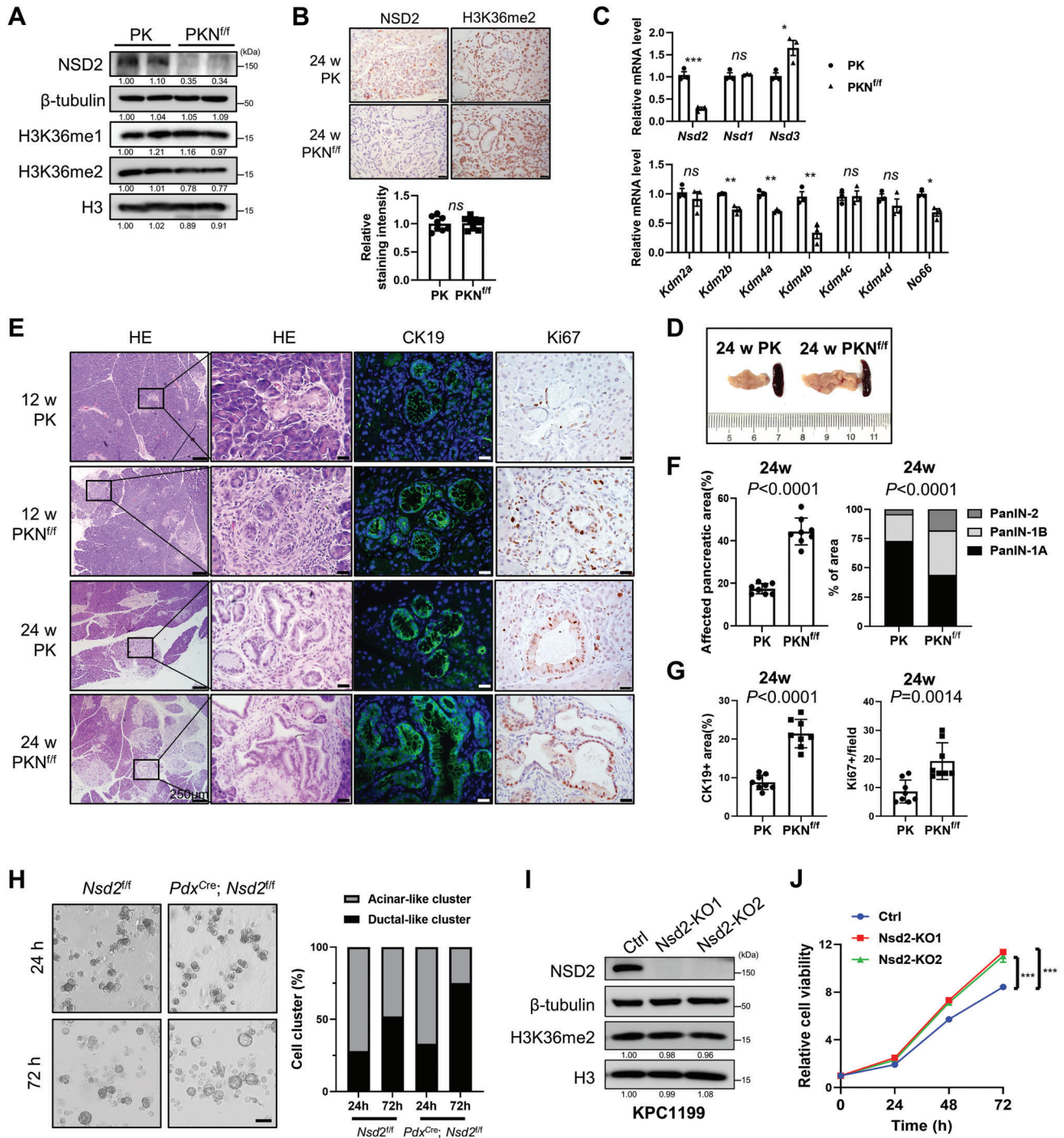ADVANCED
SCIENCE
Open Access

www.advancedscience.com

Figure 2. NSD2 loss facilitates *Kras*-induced ductal metaplasia. A) Western blotting analysis of NSD2, H3K36me1, and H3K36me2 expression in pancreas tissues of PK and PKN^f/f mice. Experiments were repeated at least three times, with similar results. B) IHC analysis of NSD2 and H3K36me2 expression in pancreas tissues of PK and PKN^f/f mice. Quantification of H3K36me2 staining intensity is shown at the bottom. Experiments were repeated at least three times, with similar results, and representative images are shown. Scale bars: 25 µm. C) RT-qPCR analysis of *Nsd2*, *Nsd1*, *Nsd3*, *Kdm2a*, *Kdm2b*, *Kdm4a*, *Kdm4b*, *Kdm4c*, *Kdm4d*, and *No66* mRNA levels of PK and PKN^f/f mice. Experiments were repeated at least three times, with similar results. D) Representative macroscopic pancreas images of indicated mice. E) Pancreatic tissues from indicated mice for staining of HE, CK19, and Ki67 (n = 8 per group). Scale bars: 25 µm. F) Quantification of affected pancreatic area (%) and the ratio of PanIN-1A, PanIN-1B, and PanIN-2 in affected pancreatic areas from indicated mice at 24 weeks (n = 8 per group). G) Quantification of CK19 positive area and Ki67 positive cells per field from indicated mice at 24 weeks (n = 8 per group). H) Representative images and statistic of acinar-to-ductal metaplasia of acinar explants from indicated mice. Experiments were repeated at least three times, with similar results, and representative images are shown. Scale bars: 50 µm. I) Western blotting analysis of NSD2 and H3K36me2 expressions in Ctrl, Nsd2-KO1 and Nsd2-KO2 cells (KPC1199 derived). Experiments were repeated at least three times, with similar results. J) CCK8 assay of Ctrl, Nsd2-KO1, and Nsd2-KO2 cells (KPC1199 derived). Experiments were repeated at least three times, with similar results.
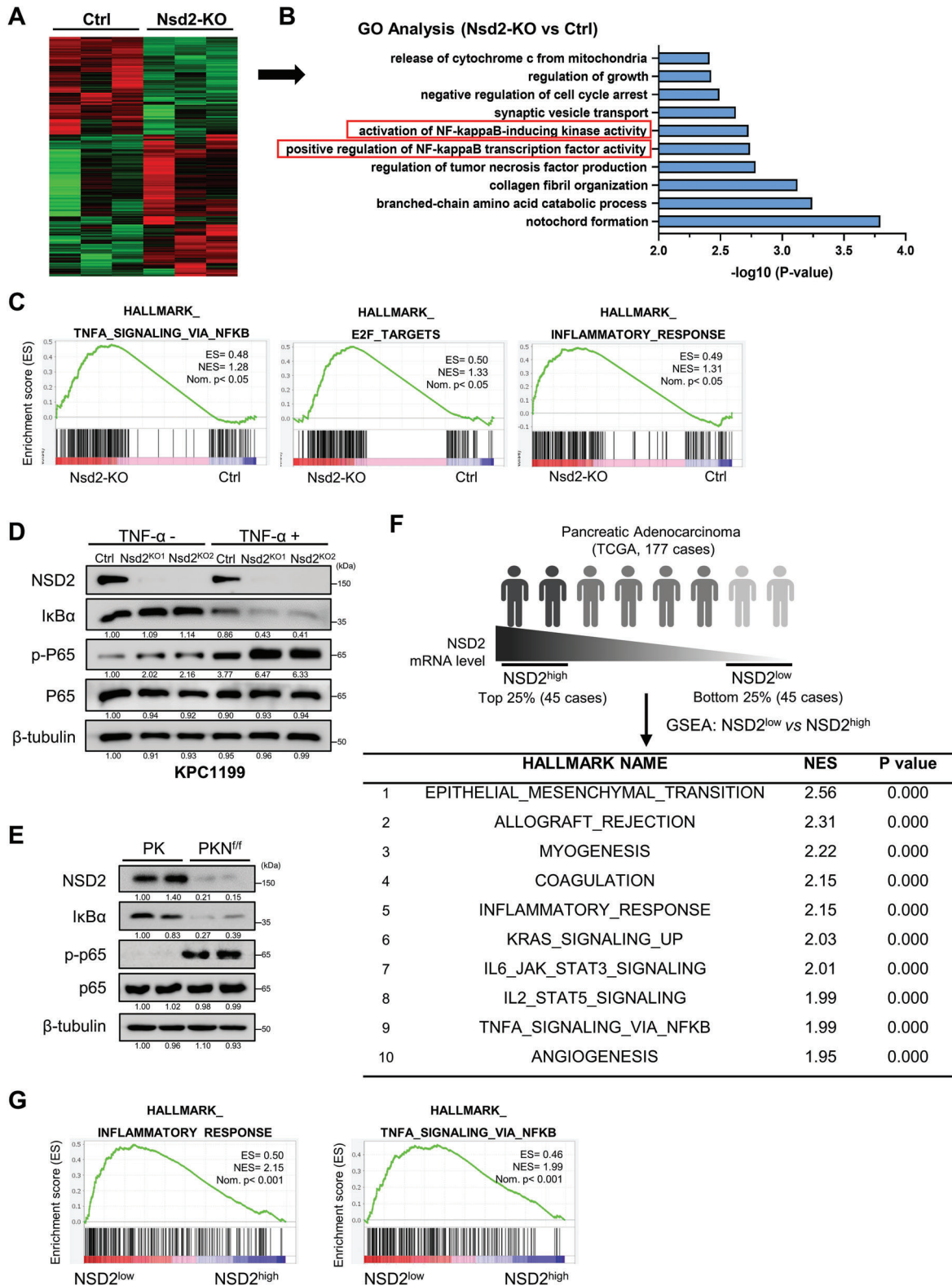
Figure 3. Loss of NSD2 activates NF-κB signaling pathway. A) Heat map of RNA-seq data to compare the gene expression of Ctrl and Nsd2-KO derived from KPC1199 cells. B) Go analysis of gene expression changes in RNA-seq data (Ctrl and Nsd2-KO). C) GSEA enrichment plots of differentially expressed genes associated with *Nsd2* deletion. D) Western blotting analysis of NSD2, IκBα, p-p65, and p65 levels in Ctrl, Nsd2-KO1, and Nsd2-KO2 cells (KPC1199 derived) treated without or with TNF-α (20 ng ml^{-1}) for 30 min. Experiments were repeated at least three times, with similar results. E) Western blotting analysis of NSD2, IκBα, p-p65, and p65 expressions in PK and PKN$^{f/f}$ mice. Experiments were repeated at least three times, with similar results.

could promote p65 nuclear translocation. According to IHC staining, more p65 proteins were accumulated in the nucleus in the pancreatic tissue of PKN$^{f/f}$ mice than in that of PK mice (Figure 4F). Moreover, compared with the Ctrl, two independent Nsd2-KO cell lines both exhibited more nuclear translocation of p65 in response to TNF-α treatment (Figure 4G). In addition, immunofluorescence (IF) analysis also revealed that loss of Nsd2 promoted nuclear translocation of p65 (Figure 4H), while NSD2 overexpression inhibits the p65 nuclear translocation under TNF-α treatment (Figure S4I, Supporting Information). These data all indicate that *Nsd2* deletion results in elevated p65 nuclear accumulation, which further demonstrates the enhanced activation of NF-κB signaling.

2.5. NSD2 Interacts with the DNA Binding Domain of p65 and Inhibits Its Transcriptional Activity

As mentioned before, *Nsd2*-deficient mice activated the NF-κB signaling pathway, while H3K36me2 was not significantly reduced (Figure 2A,B). Since both NSD2 and p65 are localized in the nucleus, we next investigated whether the activation of NF-κB caused by NSD2 depletion also resulted from the physical interaction of NSD2 with p65. The localization of NSD2 and p65 was examined by IF staining in KPC1199 and PANC1 cells treated with or without TNF-α. The data showed that p65 was translocated to the nuclei 15 min after TNF-α treatment, and the co-localization between NSD2 and p65 occurred in the nucleus (**Figure 5A**). We next assessed the endogenous interaction between NSD2 and p65 by co-immunoprecipitation (co-IP) with an anti-NSD2 antibody in KPC1199 and PANC1 cells treated with TNF-α. The results indicated that endogenous NSD2 showed an interaction with endogenous p65 (Figure 5B). Exogenous co-IP assays also showed that both NSD2 and mutant NSD2^{Y1179A} were able to bind with p65 (Figure 5C), suggesting that the protein interaction between NSD2 and p65 was independent of NSD2 enzymatic activities.

Next, we examined the NSD2-binding domain of p65 by co-IP with truncation mutants of p65 (Figure S5A, Supporting Information). Consistent with the data shown in Figure 5C, NSD2 bound to full-length p65. Furthermore, the N-terminal domain contains the DNA binding domain of p65 (p65-N1 and p65-N), but not the dimer formation domain with the activation domain (p65-N2C), coprecipitated with flag-tagged NSD2, indicating that p65 interacts with NSD2 via its DNA binding domain (Figure 5D). Consistent with the above results, the protein-protein docking analyses indicated that the Y891 residue could form hydrogen bonds with the I8 in p65, and the R956 residue could form hydrogen bonds with the M1 in p65. The interaction between NSD2 and p65 was independent of the NSD2 enzymatic activities site.

Since NSD2 interacts with the DNA binding domain of p65, we determined whether NSD2 affected the binding of NF-κB to the κB site in vitro by electrophoretic mobility shift assay (EMSA). NSD2 depletion enhanced NF-κB binding to the κB site, while NSD2 overexpression decreased it (Figure 5G). Furthermore, we

questioned whether NSD2 affected the binding of p65 to target gene promoters in vivo by ChIP-seq assays. In line with our hypothesis, p65 peaks were enriched around the gene promoter region, and NSD2 overexpression resulted in a reduction in the intensity of p65 signals (Figure 5H). ChIP–qPCR assays were used to validate the p65 bindings at the promoters of the *Ccnd1, Vegfa*, and *Ccl5*, and the results showed that the bindings of p65 to these genes were significantly decreased along with the NSD2 overexpression (Figure 5I). In addition, Nsd2 and p65 co-occupancy was also detected at the promoters of these genes (Figure S5D,E, Supporting Information).

In addition, NF-κB luciferase reporter assays were performed in 293T cells. The plasmid expressing a dominant active form of p65 (p65^{S536D}) was used to mimic phosphorylation at Ser536 of p65.[25] The results showed that NF-κB luciferase activity was significantly increased in the *Nsd2*-deficient cells but decreased in the *Nsd2*-overexpressing cells (both Nsd2^{WT} and Nsd2^{Y1179A} cells) (Figure S5B, Supporting Information). RT-QPCR further validated that the expression levels of NF-κB target genes were significantly increased in Nsd2-KO cells, including *Ccnd1, Vegfa, Ccl5*, and *Cxcl12* (Figure S5C, Supporting Information).

Collectively, these results indicate that NSD2 interacts with the DNA binding domain of p65 and inhibits its transcriptional activity.

2.6. Inhibition of NF-κB Signaling Relieves the Symptom of *Nsd2*-Deficient Mice and Sensitizes *Nsd2*-null PDAC to Gemcitabine

Given that loss of NSD2 facilitates *Kras*-induced ductal metaplasia by activating the NF-κB signaling pathway, we investigated whether NF-κB signaling inhibitors could rescue the mice from these symptoms. JSH-23 and SN-50, specific NF-κB inhibitors (NF-κBi) that directly inhibit NF-κB nuclear transport[26–31] were utilized in 12-week-old PK and PKN$^{f/f}$ mice. The compound was administered by intraperitoneal injection (i.p.) four times a week for four weeks, respectively (Figure S6A, Supporting Information). Compared with the vehicle control group, PKN$^{f/f}$ mice treated with JSH-23 or SN-50 showed much fewer ADM/PanIN lesions, while PK mice treated with JSH-23 or SN-50 only showed a relatively modest decrease in ADM/PanIN lesions area (**Figure 6B,C**). In addition, the pancreas of treated mice exhibited significantly reduced CK19 and Ki67 (Figure 6A). As expected, both JSH-23- and SN-50-treated mice displayed decreased nuclear p65 staining signals (Figure 6A) and p65 target genes expression levels (Figure S6B, Supporting Information). Hence, inhibition of NF-κB signaling relieved the symptoms caused by *Nsd2* deletion in mice.

We also treated the *Nsd2*-deficient KPC1199 cells with JSH-23 and SN-50 respectively. As shown by CCK8 assays, *Nsd2* loss promoted cell proliferation, which was significantly inhibited by treatment with either JSH-23 or SN50 (Figure 6D,E). Next, wound healing and transwell-based invasion assays showed decreased cell migration and invasion after treatment with either

---

F) GSEA analysis of gene expression between NSD2^{low} (patients with low expression of NSD2, 45 cases, 25%) and NSD2^{high} (patients with high expression of NSD2, 45 cases, 25%) from the TCGA database. The significantly enriched hallmark pathways were listed. NES, normalized enrichment score. G) Inflammatory response and TNF-α signaling via NF-κB enrichment plots in NSD2^{low} patients compared with NSD2^{high} patients are depicted.
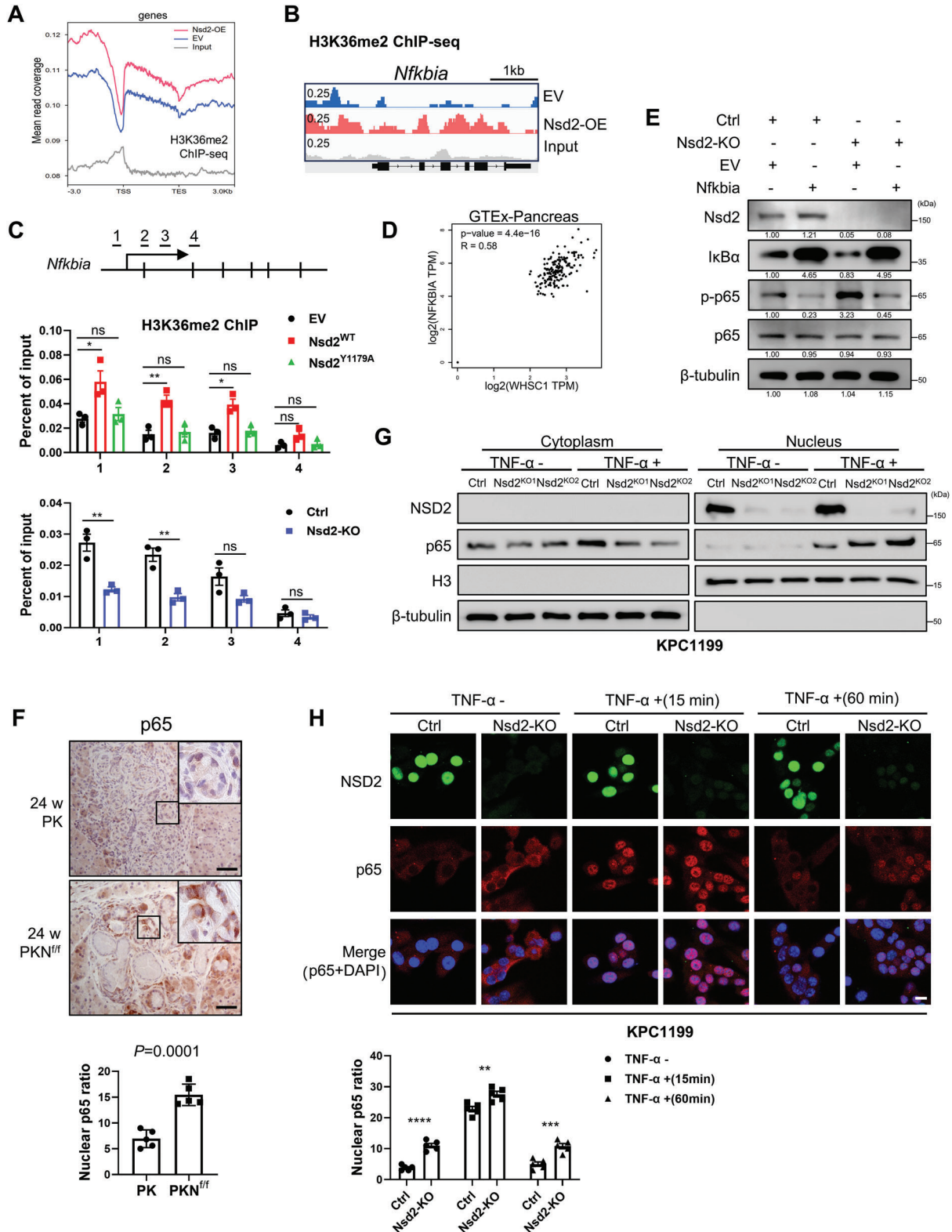
Figure 4. NSD2 promotes *Nfkbia* expression and inhibits p65 nuclear translocation. A) Normalized read density of H3K36me2 ChIP-seq signals of empty vector (EV) and NSD2-overexpressing (Nsd2-OE) cells (derived from PANC1) from 3 kb upstream of the TSS to 3 kb downstream of the TES. B) Snapshot of H3K36me2 ChIP-seq signals at the *Nfkbia* gene loci in PANC1 cells. C) ChIP-qPCR of *Nfkbia* in EV, Nsd2^WT, and Nsd2^Y1179A cells (middle). ChIP-qPCR of *Nfkbia* in Ctrl and Nsd2-KO cells (bottom). The locations of the ChIP primer pairs used were denoted as numbers (top). Experiments were repeated at least three times, with similar results. D) The Pearson product-moment pair-wise gene correlation analysis between *NSD2* (*WHSC1*)

**ADVANCED
SCIENCE NEWS**

www.advancedsciencenews.com

**ADVANCED
SCIENCE**
Open Access

www.advancedscience.com

JSH-23 or SN50 (Figure S6C,D, Supporting Information). Collectively, these results suggested that pancreatic tumorigenesis in vivo and cell proliferation in vitro due to *Nsd2* deletion are mediated by the activation of NF-κB signaling.

Next, we tested the sensitivity of Nsd2-deficient PDAC cells to chemotherapy drug gemcitabine, and no difference in gemcitabine sensitivity was observed between Ctrl and Nsd2-KO cells (Figure 6F). We further compared the sensitivity to gemcitabine with or without NF-κBi, and the results showed that Nsd2-KO cells were more sensitive to gemcitabine when NF-κB signaling was blocked with NF-κBi (JSH-23 or SN50) (Figure 6G,H). Combined treatment with gemcitabine and NF-κBi significantly reduced the viability of *Nsd2*-null PDAC cells (Figure 6G,H). Taken together, these data provide a therapeutic strategy for PDAC patients with NSD2 low/loss by combined treatment with gemcitabine and NF-κBi.

2.7. NSD2 Expression Decreased in PDAC Patients and Negatively Correlated to Nuclear p65 Expression

To characterize the clinical role of NSD2 in PDAC, we analyzed NSD2 mRNA expression in public datasets of PDAC. The results indicated that the expression levels of *NSD2* in PDAC samples were significantly lower than that in the normal pancreas (GSE15471,[32] GSE1542,[33] and GSE16515[34]) (**Figure 7A**). To further assess the clinical relevance of NSD2 in PDAC, we performed IHC analyses to determine the NSD2 level in a PDAC tissue array (Figure 7B), and the quantification results showed that the NSD2 level in the PDAC samples was lower than that in the pericarcinomatous samples (Figure 7C,D). However, there is no significant difference in H3K36me2 level between the PDAC and the pericarcinomatous samples (Figure S7A–C, Supporting Information). Taken together, the low level of NSD2 protein, rather than H3K36me2, indicates the aggressive feature of PDAC.

To delineate the clinical relevance of p65 and NSD2, we next examined the expression levels of nuclear p65 and NSD2 in PDAC patients. The results showed that the nuclear p65 level exhibited negative correlation with the NSD2 level (Figure 7F). Collectively, NSD2 expression decreased in PDAC patients and negatively correlated to nuclear p65 expression.

3. Discussion

PDAC is a clinically challenging cancer, due to both its late stage at diagnosis and its complex molecular pathology.[4] Therefore, a new understanding of the pathogenesis of PDAC can help reveal new opportunities for early detection and effective targeted therapy of PDAC. NSD2 is an important histone

methyltransferase,[15] and its oncogenic role in many cancer types has been gradually revealed in recent years.[15–17] In this study, we demonstrate that NSD2 overexpression restrains pancreatic tumorigenesis, while NSD2 loss facilitates it, by using genetically engineered mouse models (GEMMs) (Figures 1 and 2). In line with in vivo data, mouse pancreatic acinar explants assays showed the same results (Figures 1 and 2). Our results showed that NSD2 acted as a novel tumor suppressor in pancreatic cancer and revealed the multiple mechanisms by which NSD2 suppresses both p65 phosphorylation and downstream transcriptional activity during pancreatic tumorigenesis (**Figure 8**).

Recent work reported that NSD2-mediated H3K36me2 promoted EMT, tumor differentiation and metastasis in PDAC using cell lines and orthotopic implantation models.[35] However, our results demonstrated that NSD2 was a tumor suppressor during pancreatic tumorigenesis, using GEMMs models, which develop *de novo* tumors in a natural immune-proficient microenvironment, closely mimicking the histopathological and molecular features of human PDAC. Our also results showed that H3K36me2 was not significantly reduced in *Nsd2*-deficient mice, which could be due to the reduced expression of demethylases *Kdm2b*, *Kdm4a*, *Kdm4b*, and *No66*, and increased expression level of *Nsd3* (Figure 2A–C). Moreover, NSD2 is a large protein of more than 150 kDa. Apart from the evolutionarily conserved catalytic SET domain, it contains other physiologically functional domains,[36] which may play important roles in protein-protein and/or protein-DNA/RNA interaction.[37] Study reported that NSD2 can regulate the WNT signaling pathway through interaction with β-catenin.[38] NSD2 can interact with TWIST1 and then lead to an increase in H3K36me2, thus promoting the EMT.[39] What's more, interaction with NSD2 promotes SRC-3 phase separation and alters the transcriptome in myeloma cells.[40] In this study, luciferase reporter assays and exogenous Co-IP assays revealed that NSD2 interacted with p65 and inhibited NF-κB transcriptional activity independently of its enzymatic activities (using a catalytic inactivating mutation NSD2^{Y1179A} variant). As the function of NSD2 is largely dependent on its enzymatic activities, our results demonstrate that NSD2 inhibited NF-κB transcriptional activity in the nucleus by interacting with p65, which is a histone methylation-independent regulatory pathway.

During canonical NF-κB signaling, inflammatory stimulation activates the IKK complex, which phosphorylates the IκB, resulting in ubiquitination and proteasomal degradation of IκB.[41,42] The degradation of IκB releases the p65/p50 NF-κB heterodimer, allowing its nuclear translocation and promoter binding for target gene transcription.[41,42] Strict regulation of the NF-κB signaling pathway is critical for pathological inflammation and cancer development.[43] It is necessary for negative regulatory mechanisms that attenuate extensive signaling activity for the initiation and propagation of NF-κB signaling. Studies of such negative regulation of NF-κB signaling have mostly focused on the

and *NFKBIA* with GTEx-Pancreas expression database. E) Western blotting analysis of NSD2, IκBα, p-p65, and p65 levels in Ctrl and Nsd2-KO cells (KPC1199 derived) with or without Nfkbia overexpression. F) IHC analysis of p65 expression in pancreatic tissues from indicated mice at 24 weeks (n = 5 per group). Quantification of nuclear p65 mean intensity is shown at the bottom. Scale bars: 50 µm. G) Western blotting analysis of NSD2 and p65 in cytoplasmic and nuclear fractions in Ctrl, Nsd2-KO1, and Nsd2-KO2 cells (KPC1199 derived) treated without or with TNF-α (20 ng ml^{-1}) for 30 min. Experiments were repeated at least three times, with similar results. H) Immunofluorescence analysis of NSD2 and p65 expressions in Ctrl and Nsd2-KO cells (KPC1199 derived) treated without or with TNF-α (20 ng ml^{-1}) for 15 min and 60 min. Quantification of nuclear p65 mean intensity is shown at the bottom. Experiments were repeated at least three times, with similar results, and representative images are shown. Scale bars: 20 µm.
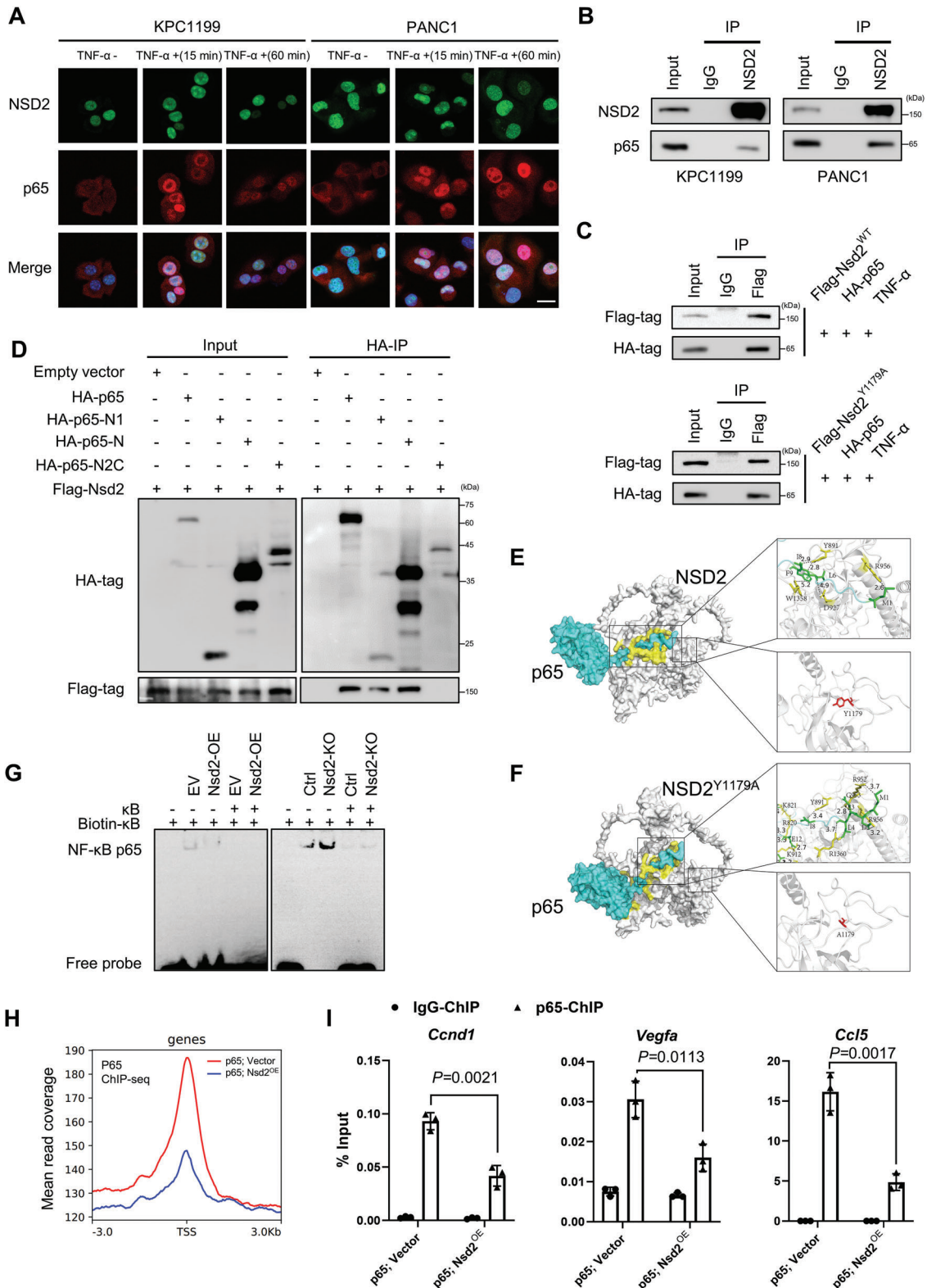
Figure 5. NSD2 interacts with the DNA binding domain of p65 and inhibits its transcriptional activity. A) Localization of NSD2 and p65 was observed by a confocal microscope. KPC1199 and PANC1 cells were treated without or with TNF-α (20 ng/ml) for 15 min and 60 min. Scale bars: 20 µm. Experiments were repeated at least three times, with similar results, and representative images are shown. B) NSD2 was immunoprecipitated from cells extracts of KPC1199 and PANC1 cells (treated with 20 ng ml^{-1} of TNF-α for 30 min) and immunoblotted with antibodies against NSD2 and p65. Experiments were repeated at least three times, with similar results. C) HEK293T cells were co-transfected with Flag-NSD2 and HA-p65 and then treated with 20 ng ml^{-1}

reversal of ubiquitination in the cytoplasm mediated by deubiquitinating enzymes such as CYLD, OTULIN, and A20.[44–49] A20 and CYLD inhibit NF-κB signaling by targeting TRAF6 upstream of IKK.[46,48] However, there are only a few reports describing negative regulators of NF-κB signaling in the nucleus. For instance, PIAS1[50] and Twist[51] can interact with p65 and repress the transcriptional activity of NF-κB. In this study, we reveal that NSD2 is another novel and physiologically important negative regulator of NF-κB in the nucleus and may act as a brake to control the NF-κB signaling.

In addition to being a histone methyltransferase, NSD2 can also methylate non-histone proteins as well. A previous study revealed that NSD2 directly methylated PTEN at K349 and enhanced the DNA damage repair ability in colorectal cancer.[52] NSD2 was found to methylate Aurora kinase A (AURKA) at K14 and K117 and mediate cell proliferation via the p53 signal pathway.[53] Another study also revealed that NSD2 methylated STAT3, which promoted the activation of the STAT3 pathway and enhanced the ability of tumor angiogenesis.[54] In this study, we performed mass spectrometry (MS) analysis and found no evidence that NSD2 directly methylated p65 (data not shown). Our results demonstrated that NSD2 regulated p65 mainly through its protein interaction with p65 and occupying the DNA-binding domain of P65. However, whether NSD2 methylates or binds to other members of NF-κB needs to be investigated in the future.

Importantly, previous studies have revealed that NSD2-catalyzed H3K36me2 participates in crosstalk with other histone marks, such as excluding H3K27me3 in lung adenocarcinoma.[24] Consistently, we found that the level of H3K27me3 was significantly increased in Nsd2-deficient mice (Figure S8A,B, Supporting Information), indicating that loss of NSD2 results in repression of gene expression. However, the role of H3K27me3 in Nsd2-deficient PDAC remains to be explored in depth.

In summary, we reveal the physiological significance of NSD2 in pancreatic tumorigenesis. NSD2 acts as a putative tumor suppressor in *Kras*-driven pancreatic tumorigenesis. NSD2-mediated H3K36me2 promotes the expression of IκBα, which inhibits the phosphorylation of p65 and NF-κB nuclear translocation. In the nucleus, NSD2 interacts with the DNA binding domain of p65, attenuating p65-mediated NF-κB transcriptional activity. Clinical data also support that the expression level of NSD2 is downregulated (Figure 7) and negatively correlated with the NF-κB target genes (Figure S3E, Supporting Information) in human PDAC. Of note, the genes related to TNFα signaling via NF-κB were significantly enriched in the PDAC patients with lower NSD2 expression (Figure 3F,G). This study reveals the multilevel regulation of NF-κB activity by NSD2 during pancreatic tumorigenesis. We have identified NSD2 as a key tumor suppressor during pancreatic tumorigenesis and as a novel negative regulator of NF-κB signaling. This study advances the understanding of the pathogenesis of pancreatic tumorigenesis and opens therapeutic opportunities for PDAC patients with *NSD2* low/loss by combined treatment with gemcitabine and NF-κBi.

4. Experimental Section

Mice: NSD2 Flox mice (Nsd2$^{f/f}$) and NSD2-overexpressing mice (Nsd2$^{OE/+}$) were generated as previously reported[20] and gifted by Prof. Jun Qin. *Pdx*^{Cre} and LSL-*Kras*^{G12D} mice were purchased from The Jackson Laboratory. These strains were interbred to generate the experimental cohorts, which include the following genotypes: *Pdx*^{Cre}; *Nsd2*$^{f/f}$ (PN$^{f/f}$), *Pdx*^{Cre}; *Nsd2*$^{OE/+}$ (PN°), *Pdx*^{Cre}; LSL-*Kras*^{G12D} (PK), *Pdx*^{Cre}; LSL-*Kras*^{G12D}; *Nsd2*$^{f/f}$ (PKN$^{f/f}$), *Pdx*^{Cre}; LSL-*Kras*^{G12D}; *Nsd2*$^{OE/+}$ (PKN°). Mice were harvested at the indicated time for pancreas histology investigation. Histological examination of *Nsd2*$^{OE/+}$, *Pdx*^{Cre}; *Nsd2*$^{OE/+}$, *Nsd2*$^{f/f}$, and *Pdx*^{Cre}; *Nsd2*$^{f/f}$ mice at 12 months of age revealed no obvious abnormalities in pancreata (Figure S1A,B, Supporting Information). The mice that lose weight by more than 20% within 1 week will be euthanized and counted as death. All mice were bred and maintained at an animal facility under specific pathogen-free conditions. Mouse experimental protocols were approved by the Renji Hospital Animal Care and Use Committee (202201027).

Human Subjects: The human pancreatic tumor microarray from Ren Ji Hospital was approved with Local Ethics Committee approval and patient consent (KY2022-036-B). Briefly, clinical parameters of patients with pancreatic cancer were collected, including age, sex, stage, pathological diagnosis, differentiation status, TNM status, and survival. None of the patients underwent preoperative chemotherapy or radiation therapy prior to surgery.

Experimental Pancreatitis Recovery Model: Experimental pancreatitis was induced by 8 hourly intraperitoneal (i.p) injections of caerulein (100 μg kg^{-1} body weight) into indicated mice for 2 consecutive days. The mice were then allowed to recover for 7 days or 18 days prior to harvesting pancreatic tissue.

Protein-Protein Interaction Docking Analysis: The NSD2, NSD2^{Y1179A}, and p65 structures were predicted using the machine learning approach AlphaFold2 (v2.0) (https://github.com/deepmind/alphafold). Predicted interaction of protein structures of NSD2 and p65 imitated by ZDOCK. All parameters for modeling were set as default values.

Western Blotting: Tissues and cells were harvested and lysed with RIPA buffer supplemented with protease and phosphatase inhibitors (MCE). The protein concentration was measured with the BCA Protein Assay (BioRad). The protein was separated by 8%–12% SDS-PAGE gels and transferred onto polyvinylidene fluoride membranes (Millipore). Membranes were blocked in 5% BSA in TBS for 1 h at room temperature and then incubated with primary antibodies overnight at 4C, washed in TBS containing 0.1% Tween20, incubated with horseradish peroxidase (HRP)-conjugated secondary antibody for 1 h at room temperature, and developed by ECL reagent (Thermo Fisher Scientific). The primary antibodies used in this study were as follows: NSD2 (Abcam, ab75359),

of TNF-α for 30 min. Flag was immunoprecipitated from cells extracts and immunoblotted with antibodies against Flag and HA. Experiments were repeated at least three times, with similar results. D) Flag-tagged NSD2 protein and HA-tagged wild-type and truncated p65 proteins were transiently expressed in HEK293T cells and then treated with 20 ng/ml of TNF-α for 30 min. HA was immunoprecipitated from cells extracts and immunoblotted with antibodies against HA and Flag. Experiments were repeated at least three times, with similar results. E) Predicted interaction of protein structures of NSD2 and p65 extracellular domain imitated by ZDOCK. F) Predicted interaction of protein structures of Nsd2^{Y1179A} and p65 extracellular domain imitated by ZDOCK. G) EMSA assay for NF-κB p65 activity in KPC1199 cells transfected with indicated plasmids. Experiments were repeated at least three times, with similar results. H) Normalized read density of p65 ChIP-seq signals in KPC1199 cells transfected with indicated plasmids. I) ChIP-qPCR analysis of p65 binding for *CCND1*, *VEGFA*, and *CCL5* promoter in KPC1199 cells transfected with indicated plasmids, and IgG was used as the control. The locations of the ChIP primer pairs used were denoted in Figure S5E (Supporting Information). Experiments were repeated at least three times, with similar results.
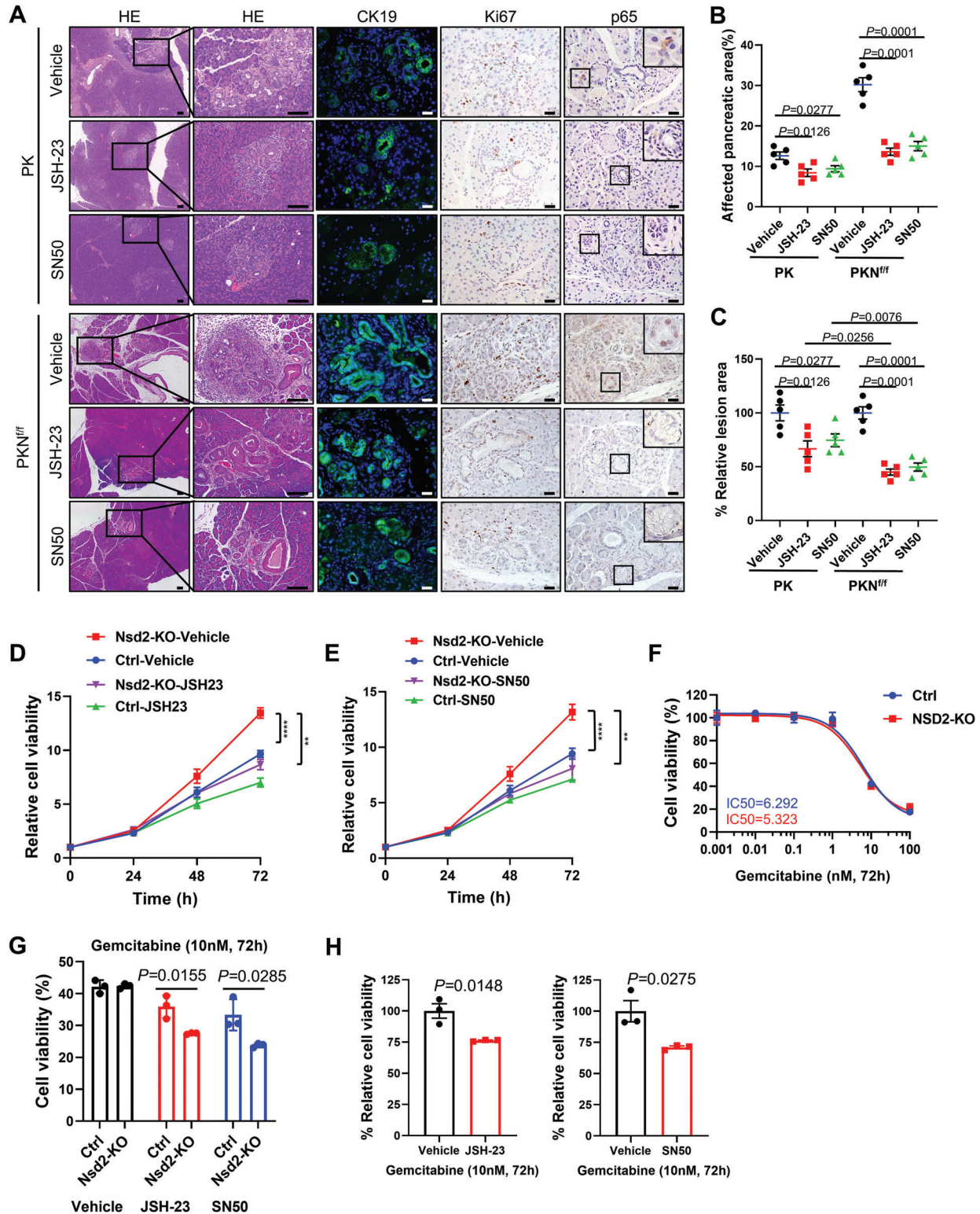
Figure 6. Inhibition of NF-κB signaling relieves the symptom of *Nsd2*-deficient mice and sensitizes *Nsd2*-null PDAC to gemcitabine. A) Pancreatic tissues from PKN$^{f/f}$ mice treated with JSH-23, SN50 or vehicle control for staining of HE, CK19, Ki67, and p65 (n = 5 per group). Scale bars: 25 μm. B) Quantification of the affected pancreatic area in PK and PKN$^{f/f}$ mice treated with JSH-23, SN50, or vehicle control (n = 5 per group). C) Quantification of relative lesions area in PK and PKN$^{f/f}$ mice treated with JSH-23, SN50, or vehicle control (compared with vehicle control) (n = 5 per group). D,E) CCK8 assay of Ctrl and Nsd2-KO KPC1199 cells treated with the NF-κB signaling inhibitor JSH-23, SN50, or vehicle control. Experiments were repeated at least three times, with similar results. F) Cell viability in Ctrl and Nsd2-KO KPC1199 cells treated with gemcitabine for 72 h. G,H) Cell viability of Ctrl and Nsd2-KO KPC1199 cells treated with gemcitabine alone or in combination with gemcitabine and JSH-23 or SN50 for 72 h.
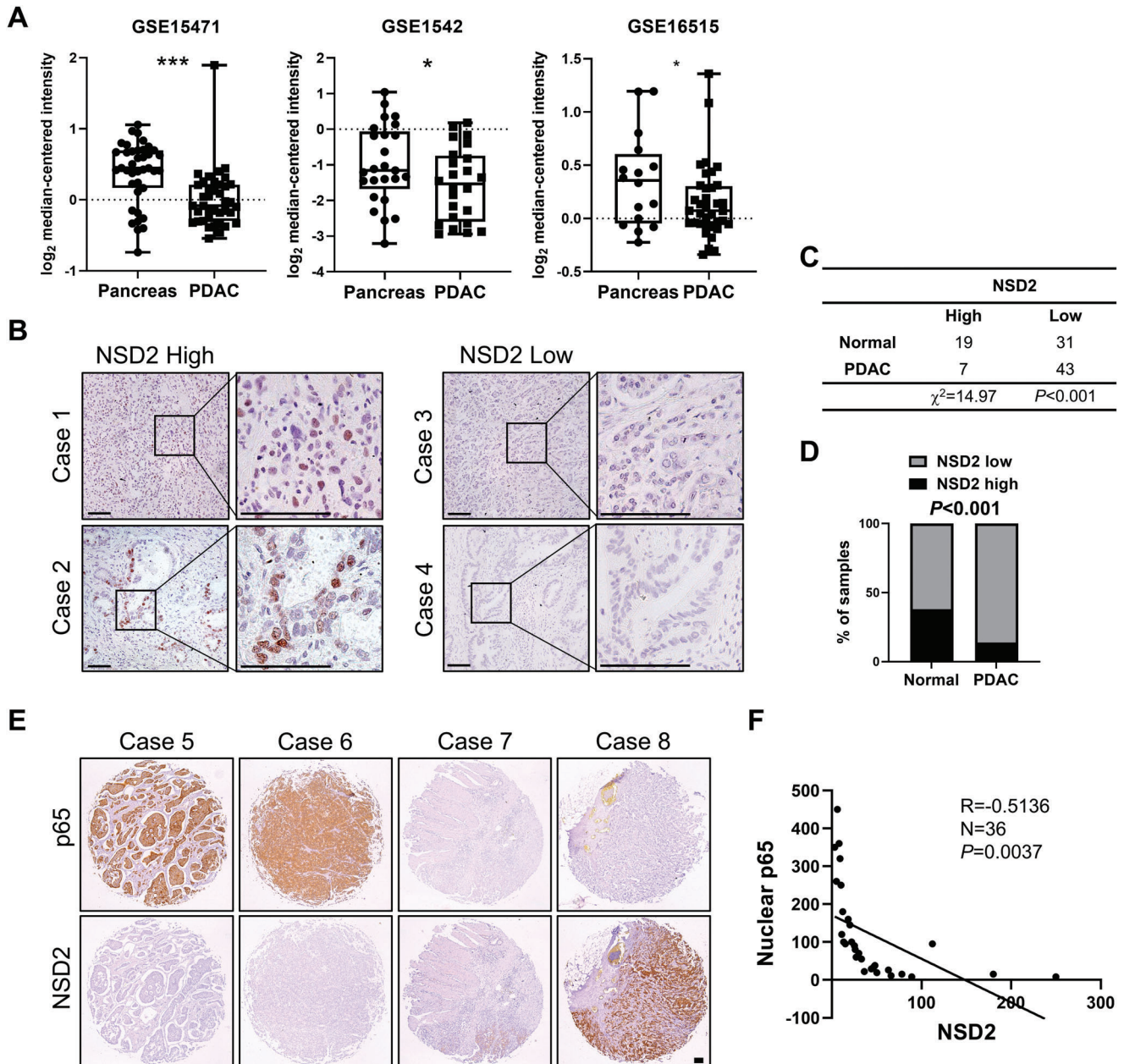
Figure 7. NSD2 expression decreased in PDAC patients and negatively correlated to nuclear p65 expression. A) Box plot of NSD2 mRNA level in pancreas controls and PDAC specimens (using dataset GSE15471, GSE1542, and GSE16515). In boxplots (middle line depicts the median and the whiskers the min-to-max range). B) Representative IHC staining indicates high and low expression of NSD2 in PDAC tissue array. Scale bars: 100 μm. C) Statistics of high and low expression of NSD2 in pericarcinomatous samples and PDAC samples. D) NSD2 expression in pericarcinomatous samples and PDAC samples is quantified (χ2 test). E) Representative IHC staining of p65 and NSD2 in PDAC tissue array. Scale bars: 100 μm. F) Correlation between nuclear p65 and NSD2 was analyzed (Pearson product-moment correlation test).

H3K36me1 (Abcam, ab9048), H3K36me2 (Abcam, ab9049), H3K36me3 (Abcam, ab9050), H3 (Cell Signaling Technology, 9715), β-Tubulin (Cell Signaling Technology, 2146), p65 (Cell Signaling Technology, 8242), p-p65(Ser536) (Cell Signaling Technology, 3033), IκBα (Cell Signaling Technology, 4814), p-IκBα(Ser32/36) (Cell Signaling Technology, 9246), IKKα/β (Abcam, ab178870), p-IKKα/β(Ser176/180) (Cell Signaling Technology, 2697).

Histology and IHC Staining: Samples were deparaffinized and rehydrated. Antigen was retrieved using 0.01 M sodium-citrate buffer (pH 6.0) at a sub-boiling temperature for 15 min after boiling in a microwave oven. To block endogenous peroxidase activity, the sections were incubated with 3% hydrogen peroxide for 20 min. After 1 h of pre-incubation in 5% normal goat serum to prevent nonspecific staining, the samples were incubated with the primary antibody against NSD2 (Abcam, ab75359), H3K36me2 (Abcam, ab9049), Ki67 (Abcam, ab6526), CK19 (Abcam, ab15463), p65 (Cell Signaling Technology, 8242) at 4°C overnight. After three washes in PBS, sections were incubated with an HRP-conjugated secondary antibody for 1 h at room temperature. Color was developed using the DAB
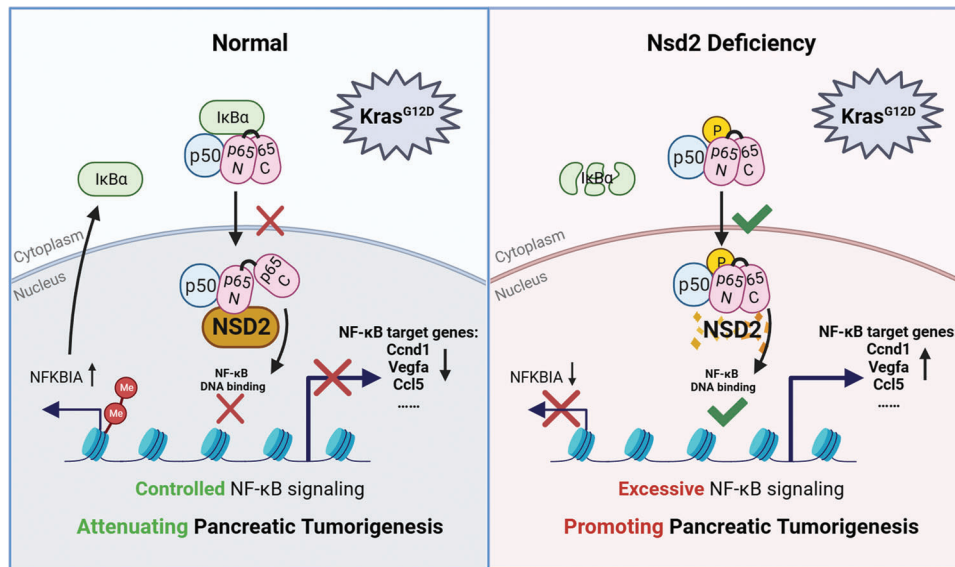
Figure 8. Multilevel regulation of NF-κB signaling by NSD2 suppresses *Kras*-driven pancreatic tumorigenesis.

(diaminobenzidine) Substrate Kit (Gene Tech). Counterstaining was carried out using hematoxylin.

Luciferase Reporter Assay: The p65 WT and p65 S536D plasmids were previously reported[25] and gifted by Prof. Helen He Zhu from the School of Medicine, Shanghai Jiao Tong University. The NF-κB firefly luciferase reporter plasmid (Bayotime, Shanghai, China) and renilla luciferase reporter plasmid were co-transfected into 293T cells using Lipofectamine 3000 (Thermo Fisher Scientific). Firefly and Renilla luciferase activities were measured using the Dual-Glo Luciferase Assay System (Promega). Renilla activity was used to normalize luciferase reporter activity. Assays were performed on cells in three wells for each experiment to obtain an average count and in three independent biological replicates.

Co-Immunoprecipitation Assays: Cells were washed with cold PBS and lysed in RIPA lysis buffer (50 mmol L^{-1} Tris-HCl, pH 8.0; 150 mmol L^{-1} NaCl; 1% NP-40) supplemented with protease and phosphatase inhibitors (Millipore) at 24 h after transfection. Cell lysates were incubated with primary antibodies overnight at 4 °C. Pierce Protein A/G Magnetic Beads (Thermo) were then added and the lysates were incubated for another 4 h at 4 °C. The immunoprecipitates were washed four times with the lysis buffer and boiled for 5 min at 98 °C in protein loading buffer. Immunoprecipitated proteins were detected by subsequent immunoblotting. Antibodies used in the co-immunoprecipitation experiments were as follows: NSD2 (Abcam, ab75359), p65 (Cell Signaling Technology, 8242), Flag-tag (Cell Signaling Technology, 14793S), HA-tag (Cell Signaling Technology, 3724).

Chromatin Immunoprecipitation Sequencing and Analyses: Cells were crosslinked with 1% formaldehyde for 10 min at room temperature and quenched with 125 mM glycine. The fragmented chromatin fragments were pre-cleared and then immunoprecipitated with Protein A + G Magnetic beads coupled with anti-H3K36me2(Abcam, ab9049) or anti-p65 (Cell Signaling Technology, 8242) antibodies. After reverse crosslinking, ChIP and input DNA fragments were end-repaired and A-tailed using the NEBNext End Repair/dA-Tailing Module (E7442, NEB) followed by adaptor ligation with the NEBNext Ultra Ligation Module (E7445, NEB). The DNA libraries were amplified for 15 cycles and sequenced using Illumina NextSeq 500 with single-end 1 × 75 as the sequencing mode. Raw reads were filtered to obtain high-quality clean reads by removing sequencing adapters, short reads (length <35 bp) and low-quality reads using Cutadapt (v1.9.1) and Trimmomatic (v0.35). Then FastQC is used to ensure high reads quality. The clean reads were mapped to the mouse genome (assembly GRCm38) using the Bowtie2 (v2.2.6) software. Peak detection

was performed using the MACS (v2.1.1) peak finding algorithm with 0.01 set as the *p*-value cutoff. Annotation of peak sites to gene features was performed using the ChIPseeker R package.

RNA-seq and Analyses: For Ctrl and Nsd2-KO of KPC1199 cells, a total of 10^7 cells were harvested for RNA preparation. Total RNA was extracted from the samples by Trizol reagent (Invitrogen) separately. The RNA quality was checked by Agilent 2200 and kept at −80 °C. The RNA with RIN (RNA integrity number) >7.0 is acceptable for cDNA library construction. The cDNA libraries were constructed for each RNA sample using the TruSeq Stranded mRNA Library Prep Kit (Illumina, Inc.) according to the manufacturer's instructions. Before read mapping, clean reads were obtained from the raw reads by removing the adaptor sequences and low-quality reads. The clean reads were then aligned to mouse genome (mm10) using the Hisat2. HTseq was used to get gene counts and RPKM method was used to determine the gene expression. DESeq2 algorithm was applied to filter the differentially expressed genes, after the significant analysis, *p*-value and FDR analysis were subjected to the following criteria: i) Fold Change >1.2 or <0.833; ii) *p*-value < 0.05. Gene ontology (GO) analysis was performed to facilitate elucidating the biological implications of the differentially expressed genes in the experiment. The GO annotations were downloaded from NCBI (http://www.ncbi.nlm.nih.gov/), UniProt (http://www.uniprot.org/), and the Gene Ontology (http://www.geneontology.org/). Fisher's exact test was applied to identify the significant GO categories (*p*-value < 0.05). Pathway analysis was used to find out the significant pathway of the differentially expressed genes according to KEGG database. The study turned to the Fisher's exact test to select the significant pathway, and the threshold of significance was defined by *p*-value < 0.05.

Acinar Cell Explants: Murine pancreas acinar cells were isolated as previously described.[55] The viability of acinar cells was examined by crystal violet staining (>95%). Primary acinar cells were seeded on precoated plates with Collagen I (5 μg cm^{-2}, YEASEN) and cultured in Waymouth medium (Gibco) supplemented with 10% FBS, 1% penicillin/streptomycin and 50 ng ml^{-1} TGFa. The ADM (acinar-to-ductal metaplasia) was observed, and representative images were taken at the indicated time.

Electrophoretic Mobility Shift Assay (EMSA):   Nuclear extracts were prepared in KPC1199 cells transfected with the indicated vector. The protein concentration from nuclear extracts was detected using the BCA Protein Assay Kit (Thermo). The sequence of biotin-labeled NF-κB p65 probes was 5′-AGTTGAGGGGACTTTCCCAGGC-3′. The DNA-binding activity of NF-

κB p65 was determined using the Chemiluminescent EMSA Kit (GS008; Beyotime) as instructed in the manufacturer's protocol.

Statistical Analysis: All experiments were performed using 3–15 mice or at least three independent repeated experiments. Unless otherwise indicated, data presented as the mean $\pm$ S.E.M. All statistical analyses were performed with GraphPad 8.0 software. Student's *t*-test assuming equal variance was used, and two-way analysis of variance for independent variance. Pearson correlation coefficients were used to evaluate the relationships between NSD2 and gene expressions. χ^2 test were used to determine whether there was a significant difference between the expected frequencies and the observed frequencies in one or more categories. *$p < 0.05$, **$p < 0.01$, and ***$p < 0.001$, ****$p < 0.0001$.

Study Approval: All animal experiments were approved by the Renji Hospital Animal Care and Use Committee (202201027). The human pancreatic tumor microarray from Ren Ji Hospital was approved with Local Ethics Committee approval and patient consent (KY2022-036-B).

Supporting Information

Supporting Information is available from the Wiley Online Library or from the author.

Conflict of Interest

The authors declare no conflict of interest.

Author Contributions

W.F. and N.N. contributed equally to this work. L.L. and J.X. designed experiment and interpreted data. W.F. performed most of the experiments; P.L., Z.C., H.R., W.Z., C.M, C.L., and Y.X. assisted in some experiments; W.-Q.G. assisted in some discussion. W.F., L.L., and N.N. wrote the manuscript. L.L., J.X., and N.N. provided the overall guidance.

Data Availability Statement

The data that support the findings of this study are available from the corresponding author upon reasonable request.

[1] W. Park, A. Chawla, E. M. O'Reilly, *JAMA, J. Am. Med. Assoc.* **2021**, *326*, 851.

[2] L. D. Wood, M. I. Canto, E. M. Jaffee, D. M. Simeone, *Gastroenterology* **2022**, *163*, 386.

[3] R. L. Siegel, K. D. Miller, H. E. Fuchs, A. Jemal, *Ca-Cancer J. Clin.* **2021**, *71*, 7.

[4] E. A. Collisson, P. Bailey, D. K. Chang, A. V. Biankin, *Nat. Rev. Gastroenterol. Hepatol.* **2019**, *16*, 207.

[5] K. Taniguchi, M. Karin, *Nat. Rev. Immunol.* **2018**, *18*, 309.

[6] M. S. Hayden, S. Ghosh, *Genes Dev.* **2012**, *26*, 203.

[7] M. Karin, Y. Ben-Neriah, *Annu. Rev. Immunol.* **2000**, *18*, 621.

[8] W. Wang, J. L. Abbruzzese, D. B. Evans, L. Larry, K. R. Cleary, P. J. Chiao, *Clin. Cancer Res.* **1999**, *5*, 119.

[9] K. Pramanik, M. Makena, K. Bhowmick, M. Pandey, *IJMS* **2018**, *19*, 3890.

[10] Y. Lu, Y.-T. Chan, H.-Y. Tan, S. Li, N. Wang, Y. Feng, *Mol. Cancer* **2020**, *19*, 79.

[11] E. Hessmann, S. A. Johnsen, J. T. Siveke, V. Ellenrieder, *Gut* **2017**, *66*, 168.

[12] K. Kawakubo, C. F. Castillo, A. S. Liss, *J. Gastroenterol.* **2022**, *57*, 819.

[13] N. Niu, X. Shen, L. Zhang, Y. Chen, P. Lu, W. Yang, M. Liu, J. Shi, D. Xu, Y. Tang, X. Yang, Y. Weng, X. Zhao, L. Wu, Y. Sun, J. Xue, *Adv. Sci.* **2023**, *10*, 2202937.

[14] S. Patil, B. Steuber, W. Kopp, V. Kari, L. Urbach, X. Wang, S. Küffer, H. Bohnenberger, D. Spyropoulou, Z. Zhang, L. Versemann, M. S. Bösherz, M. Brunner, J. Gaedcke, P. Ströbel, J.-S. Zhang, A. Neesse, V. Ellenrieder, S. K. Singh, S. A. Johnsen, E. Hessmann, *Cancer Res.* **2020**, *80*, 4620.

[15] A. J. Kuo, P. Cheung, K. Chen, B. M. Zee, M. Kioi, J. Lauring, Y. Xi, B. H. Park, X. Shi, B. A. Garcia, W. Li, O. Gozani, *Mol. Cell* **2011**, *44*, 609.

[16] I. Topchu, R. P. Pangeni, I. Bychkov, S. A. Miller, E. Izumchenko, J. Yu, E. Golemis, J. Karanicolas, Y. Boumber, *Cell. Mol. Life Sci.* **2022**, *79*, 285.

[17] R. Chen, Y. Chen, W. Zhao, C. Fang, W. Zhou, X. Yang, M. Ji, *OTT* **2020**, *13*, 6837.

[18] S. M. Foltz, Q. Gao, C. J. Yoon, H. Sun, L. Yao, Y. Li, R. G. Jayasinghe, S. Cao, J. King, D. R. Kohnen, M. A. Fiala, L. Ding, R. Vij, *Nat. Commun.* **2020**, *11*, 2666.

[19] J. J. Keats, C. A. Maxwell, B. J. Taylor, M. J. Hendzel, M. Chesi, P. L. Bergsagel, L. M. Larratt, M. J. Mant, T. Reiman, A. R. Belch, L. M. Pilarski, *Blood* **2005**, *105*, 4060.

[20] N. Li, W. Xue, H. Yuan, B. Dong, Y. Ding, Y. Liu, M. Jiang, S. Kan, T. Sun, J. Ren, Q. Pan, X. Li, P. Zhang, G. Hu, Y. Wang, X. Wang, Q. Li, J. Qin, *J. Clin. Invest.* **2017**, *127*, 1284.

[21] A. Aytes, A. Giacobbe, A. Mitrofanova, K. Ruggero, J. Cyrta, J. Arriaga, L. Palomero, S. Farran-Matas, M. A. Rubin, M. M. Shen, A. Califano, C. Abate-Shen, *Nat. Commun.* **2018**, *9*, 5201.

[22] J.-J. Wang, J. X. Zou, H. Wang, Z.-J. Duan, H.-B. Wang, P. Chen, P.-Q. Liu, J.-Z. Xu, H.-W. Chen, *Acta Pharmacol. Sin.* **2019**, *40*, 1067.

[23] C. He, C. Liu, L. Wang, Y. Sun, Y. Jiang, Y. Hao, *Cell Death Dis.* **2019**, *10*, 65.

[24] D. Sengupta, L. Zeng, Y. Li, S. Hausmann, D. Ghosh, G. Yuan, T. N. Nguyen, R. Lyu, M. Caporicci, A. Morales Benitez, G. L. Coles, V. Kharchenko, I. Czaban, D. Azhibek, W. Fischle, M. Jaremko, I. I. Wistuba, J. Sage, Ł. Jaremko, W. Li, P. K. Mazur, O. Gozani, *Mol. Cell* **2021**, *81*, 4481.

[25] C. Cheng, Z. Ji, Y. Sheng, J. Wang, Y. Sun, H. Zhao, X. Li, X. Wang, Y. He, J. Yao, L. Wang, C. Zhang, Y. Guo, J. Zhang, W.-Q. Gao, H. H. Zhu, *Theranostics* **2018**, *8*, 4633.

[26] F. Zhu, B. Zhang, J. Li, L. Zhu, *Poultry Sci.* **2020**, *99*, 2573.

[27] Z. Yu, Y. Chen, S. Wang, P. Li, G. Zhou, Y. Yuan, *Cancer Lett.* **2018**, *428*, 77.

[28] Y. Zhu, W. Zuo, X. Shen, Y. Liu, Y. Zhao, Y. Xiong, H. Cao, Y. Wang, Z. Liang, *Cell Death Discov.* **2021**, *7*, 159.

[29] B. Kunze, F. Wein, H.-Y. Fang, A. Anand, T. Baumeister, J. Strangmann, S. Gerland, J. Ingermann, N. S. Münch, M. Wiethaler, V. Sahm, A. Hidalgo-Sastre, S. Lange, C. J. Lightdale, A. Bokhari, G. W. Falk, R. A. Friedman, G. G. Ginsberg, P. G. Iyer, Z. Jin, H. Nakagawa, C. J. Shawber, T. Nguyen, W. J. Raab, P. Dalerba, A. K. Rustgi, A. R. Sepulveda, K. K. Wang, R. M. Schmid, et al., *Gastroenterology* **2020**, *159*, 575.

[30] L. Zang, F. Tian, Y. Yao, Y. Chen, Y. Shen, M. Han, Z. Meng, S. Fan, X. Zhang, T. Cai, Q. Gao, Y. Zhang, J. Lu, *J. Cell. Mol. Med.* **2021**, *25*, 5753.

[31] L.-N. Xu, S.-H. Wang, X.-L. Su, S. Komal, H.-K. Fan, L. Xia, L.-R. Zhang, S.-N. Han, *Front. Pharmacol.* **2021**, *12*, 662726.

[32] L. Badea, V. Herlea, S. O. Dima, T. Dumitrascu, I. Popescu, *Hepato-gastroenterology* **2008**, *55*, 2016.

[33] M. Ishikawa, K. Yoshida, Y. Yamashita, J. Ota, S. Takada, H. Kisanuki, K. Koinuma, Y. L. Choi, R. Kaneda, T. Iwao, K. Tamada, K. Sugano, H. Mano, *Cancer Sci.* **2005**, *96*, 387.

[34] H. Pei, L. Li, B. L. Fridley, G. D. Jenkins, K. R. Kalari, W. Lingle, G. Petersen, Z. Lou, L. Wang, *Cancer Cell* **2009**, *16*, 259.

[35] S. Yuan, R. Natesan, F. J. Sanchez-Rivera, J. Li, N. V. Bhanu, T. Yamazoe, J. H. Lin, A. J. Merrell, Y. Sela, S. K. Thomas, Y. Jiang, J. B. Plesset, E. M. Miller, J. Shi, B. A. Garcia, S. W. Lowe, I. A. Asangani, B. Z. Stanger, *Cancer Discov.* **2020**, *10*, 854.

[36] R. L. Bennett, A. Swaroop, C. Troche, J. D. Licht, *Cold Spring Harb. Perspect. Med.* **2017**, *7*, a026708.

[37] P. Xie, C. Tian, L. An, J. Nie, K. Lu, G. Xing, L. Zhang, F. He, *Cell. Signal.* **2008**, *20*, 1671.

[38] G. Toyokawa, H.-S. Cho, K. Masuda, Y. Yamane, M. Yoshimatsu, S. Hayami, M. Takawa, Y. Iwai, Y. Daigo, E. Tsuchiya, T. Tsunoda, H. I. Field, J. D. Kelly, D. E. Neal, Y. Maehara, B. A. J. Ponder, Y. Nakamura, R. Hamamoto, *Neoplasia* **2011**, *13*, 887.

[39] T. Ezponda, R. Popovic, M. Y. Shah, E. Martinez-Garcia, Y. Zheng, D.-J. Min, C. Will, A. Neri, N. L. Kelleher, J. Yu, J. D. Licht, *Oncogene* **2013**, *32*, 2882.

[40] J. Liu, Y. Xie, J. Guo, X. Li, J. Wang, H. Jiang, Z. Peng, J. Wang, S. Wang, Q. Li, L. Ye, Y. Zhong, Q. Zhang, X. Liu, D. M. Lonard, J. Wang, B. W. O'Malley, Z. Liu, *Nat. Commun.* **2021**, *12*, 1022.

[41] E. Maniati, M. Bossard, N. Cook, J. B. Candido, N. Emami-Shahri, S. A. Nedospasov, F. R. Balkwill, D. A. Tuveson, T. Hagemann, *J. Clin. Invest.* **2011**, *121*, 4685.

[42] J. Silke, L. A. O'Reilly, *Cancers* **2021**, *13*, 4510.

[43] B. Hoesel, J. A. Schmid, *Mol. Cancer* **2013**, *12*, 86.

[44] G. Courtois, *Cell. Mol. Life Sci.* **2008**, *65*, 1123.

[45] A. Kovalenko, C. Chable-Bessia, G. Cantarella, A. Israël, D. Wallach, G. Courtois, *Nature* **2003**, *424*, 801.

[46] E. Trompouki, E. Hatzivassiliou, T. Tsichritzis, H. Farmer, A. Ashworth, G. Mosialos, *Nature* **2003**, *424*, 793.

[47] K. Keusekotten, P. R. Elliott, L. Glockner, B. K. Fiil, R. B. Damgaard, Y. Kulathu, T. Wauer, M. K. Hospenthal, M. Gyrd-Hansen, D. Krappmann, K. Hofmann, D. Komander, *Cell* **2013**, *153*, 1312.

[48] H. Y. Song, M. Rothe, D. V. Goeddel, *Proc. Natl. Acad. Sci. USA* **1996**, *93*, 6721.

[49] I. E. Wertz, K. M. O'Rourke, H. Zhou, M. Eby, L. Aravind, S. Seshagiri, P. Wu, C. Wiesmann, R. Baker, D. L. Boone, A. Ma, E. V. Koonin, V. M. Dixit, *Nature* **2004**, *430*, 694.

[50] B. Liu, Y. Yang, V. Chernishof, R. R. O. Loo, H. Jang, S. Tahk, R. Yang, S. Mink, D. Shultz, C. J. Bellone, J. A. Loo, K. Shuai, *Cell* **2007**, *129*, 903.

[51] D. Šošić, J. A. Richardson, K. Yu, D. M. Ornitz, E. N. Olson, *Cell* **2003**, *112*, 169.

[52] J. Zhang, Y.-R. Lee, F. Dang, W. Gan, A. V. Menon, J. M. Katon, C.-H. Hsu, J. M. Asara, P. Tibarewal, N. R. Leslie, Y. Shi, P. P. Pandolfi, W. Wei, *Cancer Discov.* **2019**, *9*, 1306.

[53] J. W. Park, Y.-C. Chae, J.-Y. Kim, H. Oh, S.-B. Seo, *Oncogene* **2018**, *37*, 6212.

[54] D. Song, J. Lan, Y. Chen, A. Liu, Q. Wu, C. Zhao, Y. Feng, J. Wang, X. Luo, Z. Cao, X. Cao, J. Hu, G. Wang, *Oncogene* **2021**, *40*, 2952.

[55] N. Niu, P. Lu, Y. Yang, R. He, L. Zhang, J. Shi, J. Wu, M. Yang, Z.-G. Zhang, L.-W. Wang, W.-Q. Gao, A. Habtezion, G. G. Xiao, Y. Sun, L. Li, J. Xue, *Gut* **2020**, *69*, 715.

2309387 (16 of 16)